

Computational Wind Engineering for Optimal Path Planning of Unmanned Aerial Vehicles

S. Y. B. Ho*, H. Hesse* and I. H. Ibrahim*

Corresponding author: imran.ibrahim@glasgow.ac.uk

* University of Glasgow, United Kingdom.

Abstract: The current work represents an analysis of Computational Wind Engineering of a dense complex urban environment and translation of the results to optimizing the path planning for Unmanned Aerial Vehicles (UAV). Investigations into the behavior of the $k-\epsilon$ and $k-\omega$ SST turbulence models on sufficiently representative geometries were conducted. The steady-state simulations are done on the Architectural Institute of Japan (AIJ) Case B and Case F geometries. The steady-state data obtained will then need to be translated to transient data in order to better represent flow characteristics that an Unmanned Aerial Vehicles (UAV) will experience. The performance of the $k-\omega$ SST is deemed better than that of the $k-\epsilon$ model for path optimization.

Keywords: Computational Wind Engineering, Unmanned Aerial Vehicles, Turbulence Modelling

1 Introduction

With the increasing popularity of Unmanned Aerial Vehicles (UAVs), their safe operation in dense urban environments remains a critical challenge. It is expected that UAVs will operate completely autonomously in urban scenarios. Hence, there is a need to understand the behaviour of flow within the urban environment to ensure safer operation [1]. Better understanding of how the external flow affects the UAV dynamics will enable optimal path planning with increased predictability of the UAV response and therefore increase safety, efficiency and performance of UAV applications in urban settings. In addition, insights gained from understanding urban flow in complex environments can contribute towards other applications like the pedestrian wind comfort assessment [2].

The usage of Computational Wind Engineering (CWE) to assess and analyse flow characteristics is an attractive alternative to conventional wind tunnel testing due to the inherent cost, time and efficiency savings. With the rapid availability of significant low-cost computing power and rapid model prototyping, Computational Fluid Dynamics (CFD) simulations provide a fast and efficient means to simulate concurrently a large number of models. However, while CWE as a whole has become a well-established field today [3], [4] applications for CWE towards full scale and highly complex urban environments still need further work. This is evidenced by the lack of studies that address full scale complex environments likely due to the needed computational power which has only recently been made available. With regards to path planning, only one study, conducted by Murray and Anderson [1] has investigated the practical application of CWE data to path planning.

The following review provides an overview of current progress on CWE studies with sufficiently complex urban environments. The study by Hooff et al [5] on cross-ventilated flows demonstrates the recent application of CFD for CWE for simple geometries. While the study focuses predominantly on the comparison of turbulence models in prediction accuracy, the results from the simple geometry used

may not provide a good enough representation of flow behaviour for full urban environments. In another study by Hooff and Blocken [6], which investigates the indoor natural ventilation of a stadium, the surrounding geometries have been considered. The simulation results show that overheating can be an issue and that CO₂ build-up in certain areas do not meet regulatory standards depending on the wind direction. Ventilation inside the stadium was found to be significantly affected by surrounding obstacles which emphasizes the need to consider the surrounding urban environment when investigating internal flow.

In the case of external flow fields, there are several key considerations that have been the primary focus of research in CWE. The selection of turbulence modelling is a major consideration. A previous study by Mochida and Lun [7] investigated the prediction accuracy of the wind environment and thermal comfort in an urban environment using Large Eddy Simulation (LES). They concluded that LES has significantly better performance over standard and modified k- ϵ models at the time. Performance deficits in the revised k- ϵ model came in the form of over-prediction of the Turbulent Kinetic Energy (TKE). Additionally, Mochida and Lun [7] further stated that all k- ϵ models are unable to reproduce vortex shedding from buildings, over-predicted the reattachment length behind buildings and under-predicted velocity values in their wakes. These performance deficits have likely implicated the usage of LES as the preferred model to be used in CWE. Tamura [8] further demonstrated the practical usage of LES in CWE and found it to be sufficiently accurate. Thus, LES will be considered as a viable turbulence model in CWE.

However, a big drawback of LES is the computational cost as highlighted by Blocken [9] in the review of CFD for urban physics. The increasing availability of computational power can offset the computational demands of LES [8]. However, the study by Hooff et al [5] in 2017, demonstrated that the available computing power is still not viable for LES to compete with slightly less accurate models like Reynolds-Averaged Navier Stokes (RANS). The difference in computing power between LES and RANS as much as 10² orders of magnitude. Additionally, extensive best practice guidelines for LES have not been established unlike RANS where such guidelines have been developed extensively [9].

There are many variants of the RANS models besides the standard k- ϵ that have been demonstrated in CWE applications. These range from specially modified k- ϵ turbulence models [10] like Re-Normalised Group (RNG) k- ϵ and Chen-Kim k- ϵ [11] to the Wilcox k- ω model and its coupling with a modified definition of the eddy viscosity to form k- ω SST [12] as presented in detail in [3], [6]. The computational cheaper RANS models, and in particular the steady RANS variants of k- ϵ , are the most commonly used turbulence models despite their drawbacks [3].

The AIJ working group has done extensive work in the field of CWE where they have conducted a combination of wind tunnel, field measurements and CFD simulations to give extensive data for uses ranging from verification to validation [4], [10]. Critically, within the studies conducted by AIJ, the availability of a sufficiently complex geometry, Case F (Shinjuku) is available along with experimental data. The AIJ projects [10] have also shown experimentally that k- ϵ underestimates the wind speed in the wake region of buildings since k- ϵ is unable to reproduce vortex shedding. Hence, this project will study the applicability of other turbulence models for complex urban environments as studied in the AIJ project. From the conclusions of the work by Hooff et al [5], the k- ω SST will be primarily evaluated in this paper. Table 1 shows an overview of CFD studies that use the k- ω SST model. Although the list is not exhaustive, there is a lack in literature to demonstrate the validity of k- ω SST models for highly complex and dense urban environments like the AIJ Shinjuku geometry. In terms of external flow fields, only the review by Blocken et al [13] evaluating the accuracy of wind tunnel and CFD techniques for studies on wind comfort is relevant. However, the review only provides a general consensus that less expensive techniques like RANS, which includes the k- ω SST, model may be sufficiently accurate.

Table 1: A non-exhaustive list of various CWE studies using the $k-\omega$ SST turbulence models.

Author	Year	Case Study	Agreeability of $k-\omega$ SST	Ref.
Blocken et al.	2016	Includes various case studies	Supports continued use of less expensive techniques ($k-\omega$ SST)	[13]
Hu et al.	2005	Cross-ventilation between outdoor and indoor spaces	Able to sufficiently predict flow features	[14]
Peren et al.	2014, 2015, 2016	Generic Isolated building with asymmetric openings for cross-ventilation	$k-\omega$ SST provides the best prediction and is used for all analysis types	[15]–[18]
Ramponi & Blocken	2012	Generic Isolated buildings for cross-ventilation	$k-\omega$ SST provides the best prediction (computational parameters & validation study)	[19], [20]

This paper will focus on the comparison of $k-\omega$ SST with the more commonly used $k-\epsilon$ model for CWE studies of large, highly compact and dense urban environments. The accuracy of $k-\omega$ SST coupled with its less expensive computational demand make it a prime candidate for complex CWE simulations where more accurate models like LES are too computationally expensive. We will firstly evaluate the turbulence models in terms of accuracy for sufficiently complex urban environments. In addition to the investigation of the $k-\omega$ SST model, this work will also analyse the potential inaccuracies of $k-\epsilon$ by comparing the CFD results to the experimental data from the AIJ project [10].

The aspect of the paper addresses the computational cost to enable the practical application of CWE for path planning of UAVs. Following the approach in [1], steady state CFD data can be converted to a transient flow representation using the flow TKE values as an input for stochastic models of continuous wind turbulence. These transient results can be applied as gust loads to the UAV dynamics which allows better prediction in UAV path optimization without the need to run computationally expensive transient simulations, thus saving significant computational cost.

In short, the objectives of this work can be defined as:

- 1) Investigate the performance of the $k-\epsilon$ and $k-\omega$ SST turbulence models for flow over a sufficiently complex urban environment for future CWE studies.
- 2) Translation of steady-state CFD data to transient flow representation for UAV path optimization.

The remainder of the paper will firstly introduce the CFD methodology and its validation to accurately simulate the flow around complex urban environments followed by numerical studies in Section 3 that compare the performance of different turbulence models for such urban settings. The paper concludes with an overview on how the CFD data can be applied to UAV path planning.

2 Methodology

This section will introduce the implementation of the CWE simulation environment using SimScale, a cloud-based simulation platform using OpenFOAM. SimScale provides a graphical user interface where important aspects such as meshing, simulation and post-processing can be done in a browser with no need for local software. The availability of large and accessible computing power is a key advantage especially in performing complex CWE simulations. OpenFOAM is an open source numerical solver that is the primary solver used by SimScale. The usage of SimScale as a simulation platform and the implementation of simulation parameters as well as boundary conditions will be validated in this section against the experimental data by AIJ [10].

2.1 Geometry and computational grid

In this work we aim to demonstrate the applicability of $k-\omega$ SST for a hierarchy of model complexities. Due to the availability of experimental, this paper demonstrates the implementation of the CWE environment for the following AIJ benchmark test cases with growing modelling complexity [10]:

1. The AIJ benchmark test case B 4:4:1 shape building model
2. The AIJ benchmark test case F building complexes with complicated building geometry representing the actual urban area (Shinjuku)

For both benchmark test cases, the geometry is obtained directly from the AIJ [10] CFD guide website and can be seen in Figure 1. The selected test cases represent complex urban scenarios with availability of experimental data and original source files for the geometries to ensure accuracy. The AIJ Case B, while not a complex urban geometry, will be analysed to perform an initial verification of the platform as presented in Section 2.4.

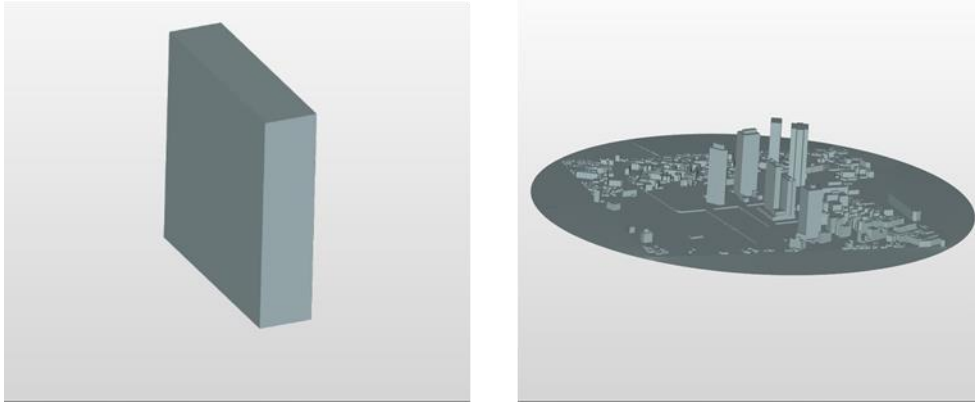


Figure 1: AIJ Case B isolated building geometry (left) and Case F (Shinjuku) geometry (right) [10].

For the computational domain size, we follow the recommendations in Refs. [9]-[21] to use the directional BR criteria for determination of domain size in addition to the Type 1 guidelines [9]. Type 1 guideline is the requirement for a fixed minimum distance between the geometry and the boundary. The set of criteria used in this case is stricter than those used by COST [22] and AIJ [4]. Similar guidelines will be applied to the Case B geometry as well but as the geometry is simple, computational cost can be saved by simply adhering to a minimum distance from the inlet to the geometry. The length and height of the domain size for the complex geometry of AIJ Case F (Shinjuku) are given by

$$BR_L = \frac{L_{building}}{L_{domain}} \leq 17\% \quad \text{and} \quad BR_H = \frac{H_{building}}{H_{domain}} \leq 17\% \quad (1)$$

The resulting domain dimensions are shown in Table 2.

Table 2: Domain length calculations for AIJ Case F (Shinjuku).

Geometry	AIJ Case F (Shinjuku)
X Length (m)	1070
Y Length (m)	1010
Z Length (m)	225
Directional BR X (%)	16.98
Directional BR Y (%)	16.95
Directional BR Z (%)	16.79
Domain X Length (m)	6300
Domain Y Length (m)	5960
Domain Z Length (m)	1340

The computational grid is created using the Hex-Dominant Parametric mesher in SimScale which utilizes SnappyHexMesh, an iterative mesh builder, to create a hexahedral unstructured mesh. The mesh has been refined at the areas in front of the geometry of the inlet and where the geometry itself is located. The level of fineness is adjusted in order to achieve three different grids for the mesh convergence study with a factor of 1.5 times between meshes [9]. The mesh convergence results are presented in Section 2.4.

2.2 Boundary conditions

The boundary conditions used in the simulations aim to replicate the experimental setup of the test cases from AIJ [10]. For the inlet, a fixed logarithmic inlet profile is used as provided by AIJ for both Cases B and F. The corresponding TKE is also provided but only for Case F. Data for the turbulence dissipation ε and specific turbulence dissipation rate ω are calculated separately from the available inlet data.

The AIJ Case B isolated building geometry, as seen in Figure 1, is simulated with the selected turbulence model of $k-\omega$ SST and standard $k-\varepsilon$ for comparison. The simulation type is incompressible and at a steady-state. The power-law velocity inlet is defined by AIJ [10] is replicated as the inlet of the simulation and is shown in Figure 2. The remaining boundary conditions and solver settings are identical to that of Case F as elaborated next.

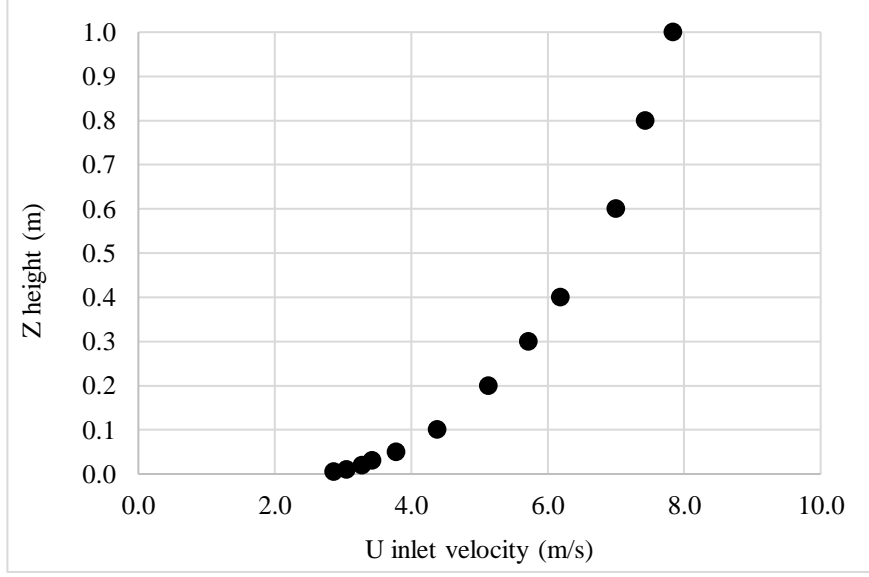


Figure 2: Inlet velocity profile for Case B.

For Case F, the inlet reference velocity of 7.8 m/s at a height of 500 m is obtained from AIJ [10]. To deduce the inlet profile for the simulations, we follow the equations also provided by AIJ. The inlet velocity is given as,

$$U(z) = \frac{u_{ABL}^*}{\kappa} \ln\left(\frac{z + z_0}{z_0}\right) \quad (2)$$

where κ is the model constant of 0.4 provided by AIJ [10]. The TKE is found as,

$$k(z) = \frac{u_{ABL}^{*2}}{\sqrt{C_\mu}} \quad (3)$$

with the atmospheric boundary layer friction velocity given as

$$u_{ABL}^* = \frac{\kappa U_h}{\ln\left(\frac{h + z_0}{z}\right)} \quad (4)$$

From Blocken [5] we can calculate ω as

$$\omega(z) = \frac{\varepsilon(z)}{C_\mu k(z)} \quad (5)$$

with

$$\varepsilon(z) = \frac{(u_{ABL}^*)^3}{\kappa(z + z_0)} \quad (6)$$

The simulation inputs for the inlet profile against height have been plotted in Figure 3 and Figure 4 for demonstration.

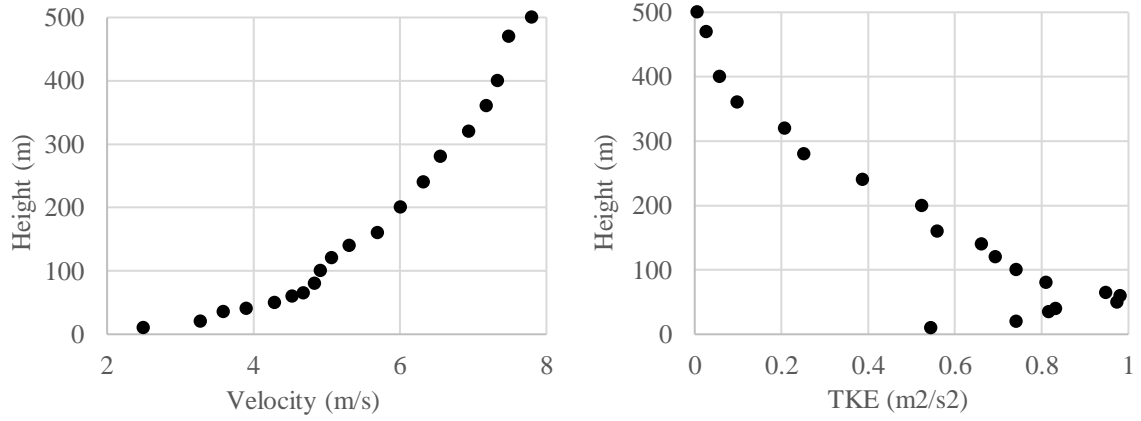


Figure 3: Velocity Profile (left) and TKE profile (right) at inlet for AIJ Case F (Shinjuku).

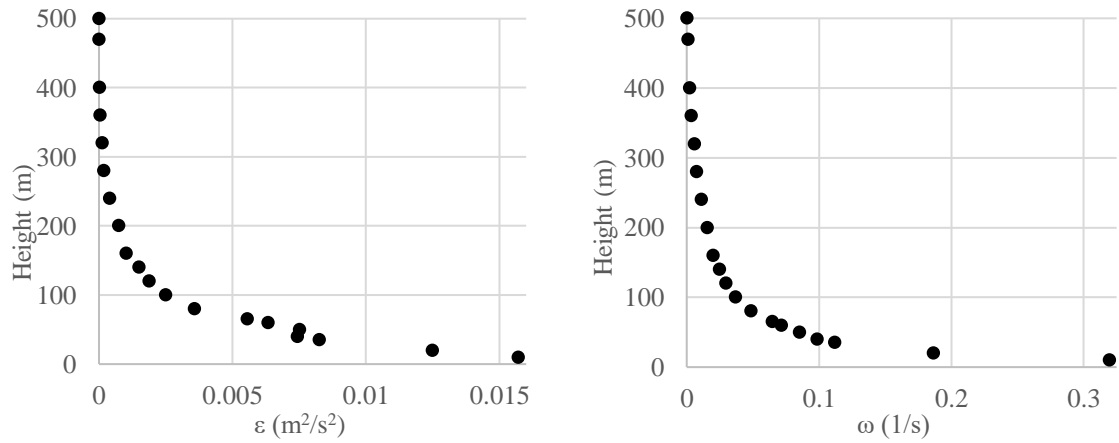


Figure 4: Turbulence dissipation profile (left) and specific turbulence dissipation profile (right) at inlet for AIJ Case F (Shinjuku).

For the sides and top of the domain, a symmetry boundary condition is used. The symmetry boundary condition applies a zero flux, a velocity normal component of zero and all normal components of all other variables as zero. For the outlet of the domain, a static gauge pressure outlet is defined and set to zero. The geometry boundary condition is set as a no-slip wall coupled with a wall function that allows a coarser mesh to be used near wall regions. For the floor, the velocity and pressure gradients are set to zero while the TKE, ε and ω are wall functions. Wall roughness is also activated where the roughness height Z_0 is 0.00018 for Case B and 0.024 for Case F following documentation from AIJ [10]. The assignments of the boundary conditions can be seen in Figure 5.

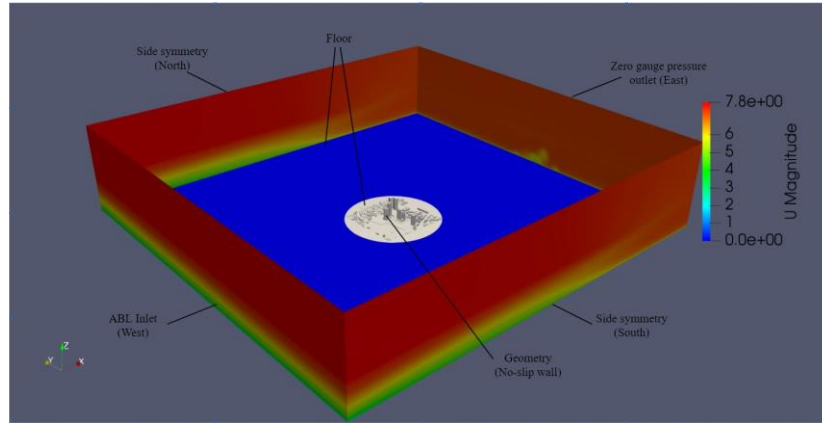


Figure 5: Visual representation of the boundary conditions for AIJ Case F at the end of the simulation.

2.3 Solver settings

The solver utilized in the investigations is the Semi-Implicit Method for Pressure-Linked Equations (SIMPLE) algorithm as flow is steady-state and incompressible. The fluid domain is air with a Newtonian viscosity model. The density is 1.225 kg/m^3 with a kinematic viscosity of $1.478\text{E-}05 \text{ m}^2/\text{s}$.

For the numerical control schemes, the pressure-based scheme is Generalised Geometric-Algebraic Multi-Grid (GAMG) and for the velocity, TKE and specific turbulence dissipation rate ω , the Preconditioned Bi-Conjugate Gradient (PBiCG) scheme is applied. These are the default solver scheme settings and are used as they have a good balance of stability and convergence speed in practice. The solution for pressure is also under-relaxed with the default value of 0.7 reduced to 0.3 in order to achieve better convergence for the pressure residuals at the cost of increased time to converge. The iterative convergence criteria is set to $1\text{E-}5$ as mentioned by Blocken [9] where at least four orders of magnitude is recommended. Due to the nature of the mesh, second order discretization schemes are not able to be used due to insufficient grid quality which brings about instability.

The simulation settings for the incompressible flow are set for an end time of 6000 with a timestep of 1. The potential flow is initialized in order to speed up convergence and increase stability of the simulation. The simulation is also done on 96 computing cores in the cloud on the SimScale platform and a scotch decomposition algorithm is used to split the processing tasks in order to simulate in parallel across all computing cores. Force plots on several surfaces of the geometry are tracked to ensure steady-state is reached and a convergence graph is produced upon the start of the simulation.

2.4 Mesh convergence study and Validation

A mesh convergence study is performed to ensure that the mesh used is optimal in terms of cell count and accuracy. The comparison point used for the Case B geometry is the velocity profile at various points along the length of the domain as seen in Figure 6. The points are at 0m, 0.025m and 0.05m from the centre point of the geometry. For Case F, comparison points are between the normalized velocity ratios at the points of interest. The location of the points is depicted in Figure 7.

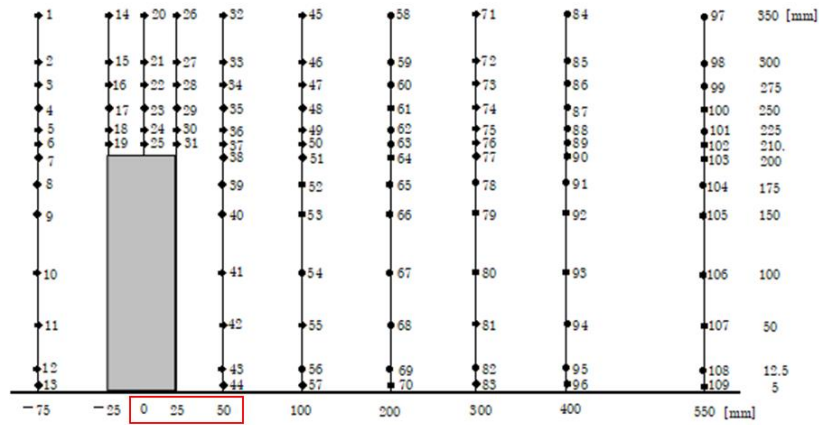


Figure 6 Points of interest for horizontal view of AIJ Case B [10].



Figure 7: Location of points of interest on AIJ Case F geometry [10].

For Case B, 3 meshes are created that are approximately 1.5 times finer than the previous mesh. The coarse mesh contains 366425 cells, fine mesh 582674 cells and finest mesh 821914 cells. Shown in Figure 8 is the velocity profiles across the points of interest. The deviation of the results for all meshes are less than 5%. However, the deviation between the fine and finest mesh is less than 1% despite a slightly higher cell count and thus will be primary mesh used.

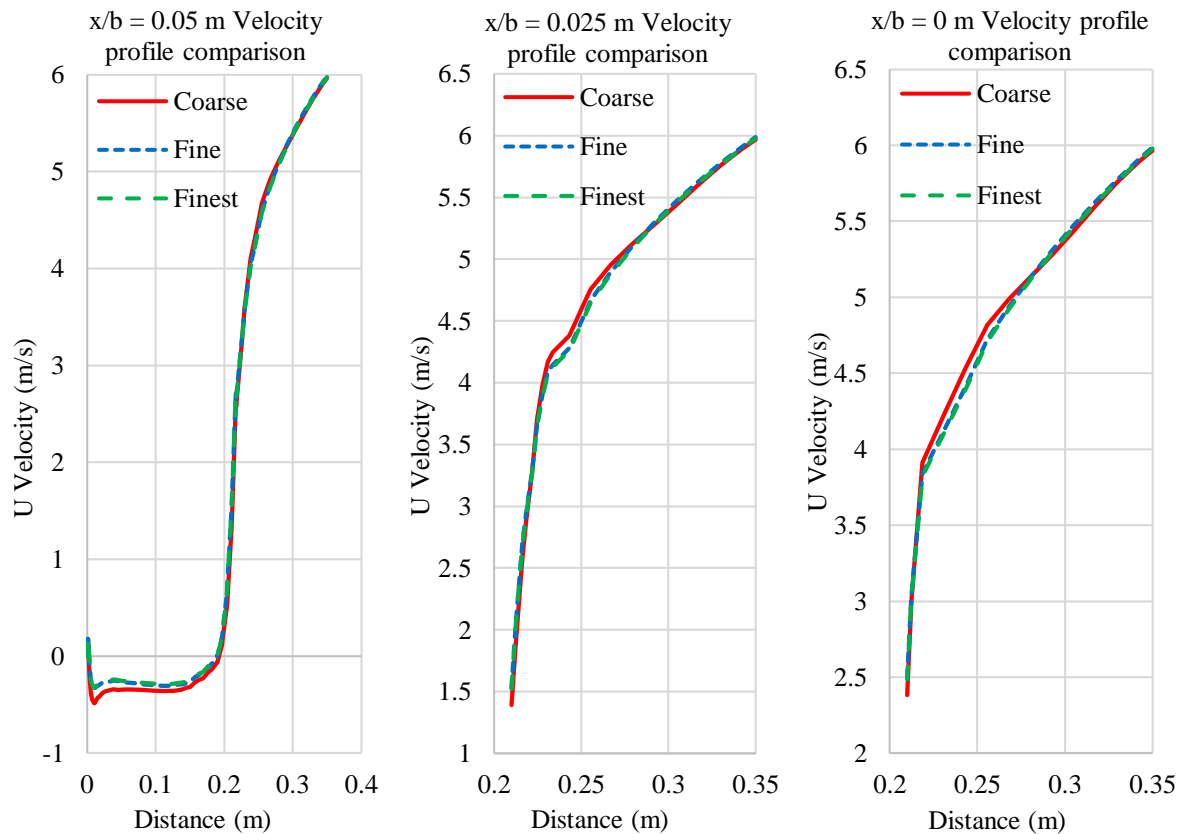


Figure 8: Velocity profiles for Case B for coarse, fine and finest meshes.

Since a non-typical simulation software is used for this investigation, validation of the solver is needed. This is done by comparing steady-state results from Case B with the experimental results provided by AIJ. The results are shown in Figure 9. From the results, the solver is deemed as verified and sufficiently accurate for continued usage. Both turbulence models also seem to agree well with the experimental results.

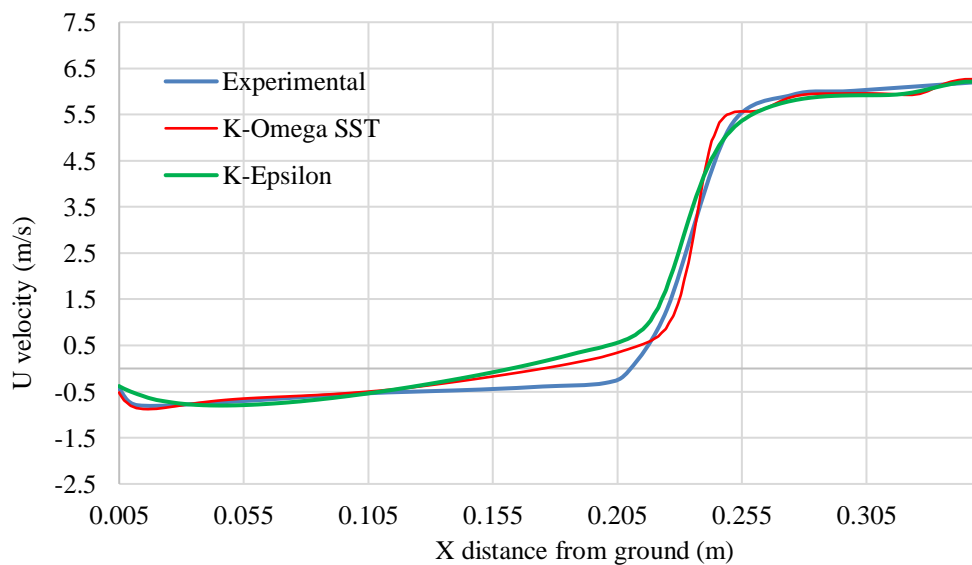


Figure 9: Velocity plot at $x/b = 0.05m$, for Case B comparing experimental data [10] versus $k-\omega$ SST and $k-\epsilon$ results.

For Case F three meshes are also created that are approximately 1.5 times finer than the previous mesh. The coarse mesh contains 23.69 million cells, the fine mesh 38.46 million cells and the finest mesh 55.7 million cells. The normalized velocities at the points of interest based on the available data, points 1 to 15, are tabulated along with the various percentage differences in Table 3. It should be noted that points 4 and 12 are the points for velocity normalization and are not included. In this case, the velocity is normalized with point 4 (point C) and point 12 (point D) as stated in AIJ's documentation [10].

Table 3: Differences for the Normalized Velocity Ratio (For Course/ Fine and Finest Mesh).

Points (Case F Velocity Ratio)	Normalized C % Difference (Coarse/Fine)	Normalized D % Difference (Coarse/Fine)	Normalized C % Difference (Fine/Finest)	Normalized D % Difference (Fine/Finest)
1	10.18	9.87	31.26	22.18
2	29.43	29.87	58.38	61.26
3	22.94	22.68	34.81	25.48
5	0.54	0.88	18.91	24.52
6	43.36	43.17	167.83	149.30
7	8.19	8.56	9.98	16.21
8	7.05	7.42	9.72	2.13
9	18.40	18.81	7.60	13.99
10	29.85	30.30	46.71	50.40
11	2.31	2.66	13.21	5.38
13	3.17	2.84	2.40	4.69
14	11.36	11.05	32.73	23.54
15	7.72	8.09	16.69	22.46

From the mesh convergence study, there is significant result deviation at several points. The deviation between the fine and finest mesh is much larger than that between the coarse and fine mesh. As such, the coarse and fine mesh will be mainly considered to be usable. While points 2, 3, 6, 9 and 10 have deviations of than 20%, the complexity of the geometry means that keeping these points within deviation is difficult. Thus, special attention needs to be paid to these points when the final results are considered. The mesh to be used will be the fine mesh as it provides a good compromise between result accuracy and computational cost.

3 Results and Discussion

3.1 Comparison of turbulence model for Case F

To evaluate the accuracy of the $k-\omega$ SST and $k-\varepsilon$ models for the complex urban Case F [10], we compare the velocities at the points of interest as defined in Figure 7. The velocities normalized by point C in order to form comparative data with the experimental results from AIJ. The points of interest including normalization points C and D are marked shown in Figure 7. It should be noted that while more points beyond 15 do exist in the AIJ experimental data, for the flow progressing from west to east, only points 1 to 15 and ratios normalized by point C contain the standard deviation data for the velocity ratio. Hence, only those points with available data will be considered in this work. All points with exception of the normalization points C and D are 10m above the ground.

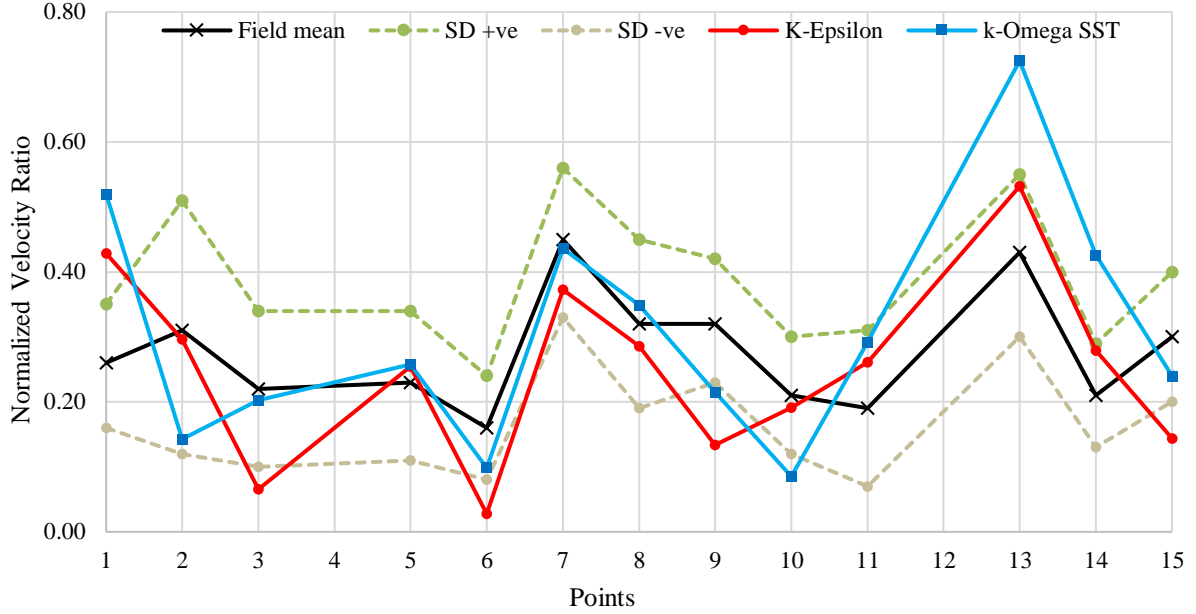


Figure 10: Comparison of the west inlet normalised by Point C for the different turbulence approximations against experimental results for AIJ Case F [10].

The resulting normalized velocities for the first 15 points of interest are compared in Figure 10 against experimental results. Points that are below the field mean and outside the standard deviation range are deemed as underpredicted. Likewise, points above the field mean indicate overpredicted results. From the literature review, it has been identified that the $k-\epsilon$ underperforms in wake prediction. This is reinforced in the current study by examining the data at point 3, 6, 8, 9 and 15 where the $k-\epsilon$ model underpredicts the velocities as compared to the $k-\omega$ SST model. At points 3, 6 and 15, the underprediction has caused the velocity to be out of acceptable margin compared to the experimental data.

Regarding overprediction, the $k-\epsilon$ model performs better in general where only point 1 is overpredicted (out of margin) while the $k-\omega$ SST model overpredicts (out of margin) the velocity at points 1 and 13. For both points, it has been examined that the over-prediction is likely due to poor mesh quality in the regions around points 1 and 13.

Finally, to evaluate the accuracy of both turbulence models to capture the flow in this complex urban environment, we compare the number of points where the velocity predictions outside the margins of standard deviation. For the $k-\epsilon$ model, there are five points out of margin (1, 3, 6, 9, 15) with point 1 overpredicting and the remaining points underpredicting. The $k-\omega$ SST model tends to overpredict the velocity profile with points 1, 13 and 14 overpredicting while points 9 and 10 underpredict the results.

Performance of the two turbulence models can be deemed similar with regards to accuracy. However, in the use case of UAV path optimization, overprediction is more desirable as regions of strong wind flow can be identified and compensated for in a conservative manner. This is in contrast to underprediction where incorrectly captured adverse flow gradients can lead to critical and poor UAV performance. Despite several deficits in prediction for the AIJ Case F benchmark test, we consider the $k-\omega$ SST model the better approach for CWE of urban environments, especially in the context of safe path planning for UAVs in an urban setting.

3.2 Application to UAV path optimization

In the final section we demonstrate how the CWE results for urban environments can be used for optimal path planning in UAV applications. By analysing the CFD simulation results at different heights throughout the entire domain, we can determine areas where strong velocity gradients or high turbulence occur in order to compensate for the continuous turbulence effects or avoid such areas entirely. Here, we consider the approach by Murray and Anderson [1] which models the response of a UAV to determine its safe operating limit as a function of the flow TKE values. Once a TKE limit has been determined for a specific UAV design, the CWE results can be used to determine optimal or safe paths for the UAV to operate. Figure 11 shows an example of such a manual path planning exercise through the AIJ Case F geometry by simply avoiding regions of high TKE. However, based on computed TKE values for different wind directions, the process can be automated using model-based optimisation methods for 3D path planning of UAVs [23].

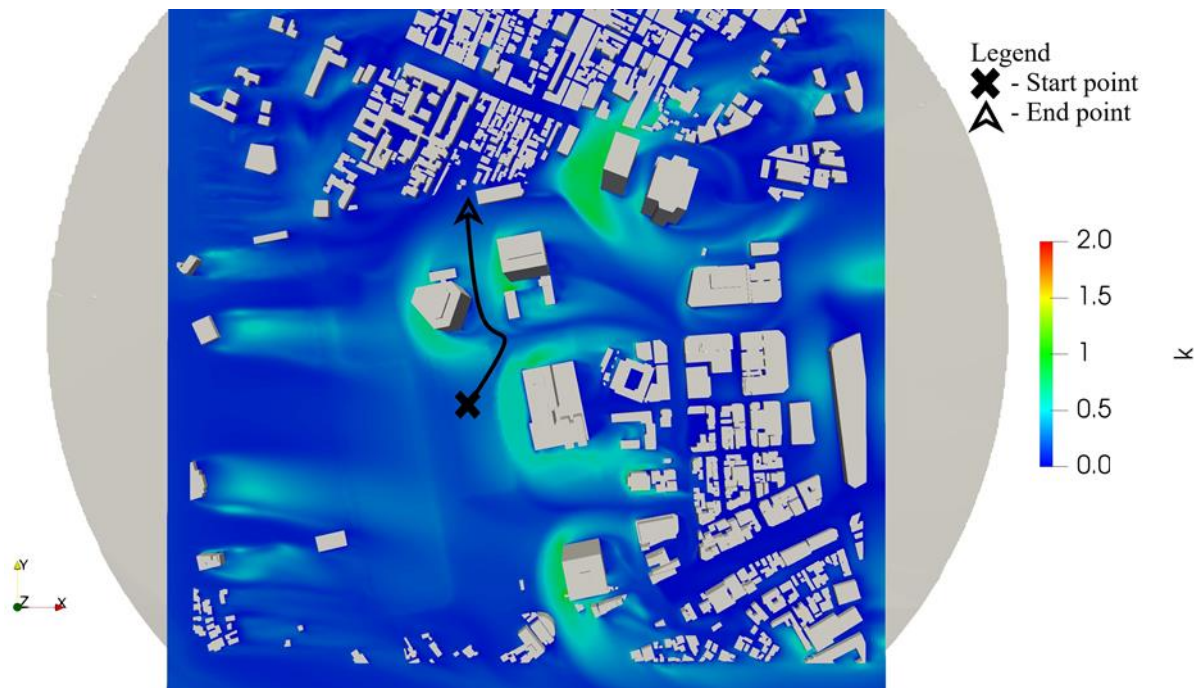


Figure 11: TKE contour at 10m for AIJ Case F geometry [10] with a sample UAV path.

The steady-state results, as shown in Figure 11 are a good indicator of possible areas of high flow gradients, but the results are not able to sufficiently replicate transient disturbances over time. While a possible solution to this lack of data would be a transient simulation of the complex geometry, with current computational resources it is still too expensive due to the large number of cells involved in a typical urban flow study. Instead, Murray and Anderson [1] propose a method based on stochastic wind turbulence models to approximate the transient flow behaviour based on steady-state CFD results.

Atmospheric turbulence is typically modelled as a stochastic process in classical flight simulation. The continuous von Kármán and Dryden turbulence models are the most established turbulence representation in flight simulation and aircraft certification to evaluate the effects of continuous gust disturbances on the aircraft flight behaviour [24]. Similar approaches have also been applied to gust modelling on large wind turbines [25] and, recently, also on the gust response of UAVs in urban airspaces [1].

Following the example in [1] and the standard approach in Matlab [26], we consider the Dryden spectrum to model the transient wind behaviour and obtain a temporal representation of the flow around urban environments. Based on the Dryden turbulence model [26], the spectra for disturbance velocities in longitudinal, lateral and vertical directions are defined as

$$\Phi_{u,v}(\omega) = \sigma^2 \frac{2L}{\pi V} \frac{1}{\left(1 + \left(\frac{L\omega}{V}\right)^2\right)^2} \quad (7)$$

$$\Phi_w(\omega) = \sigma^2 \frac{L}{\pi V} \frac{1 + 3\left(\frac{L\omega}{V}\right)^2}{\left(1 + \left(\frac{L\omega}{V}\right)^2\right)^2} \quad (8)$$

where u, v and w represent the longitudinal, lateral and vertical velocity contributions. In typical certification requirements [27], the turbulence intensities $\sigma_{u,v,w}$ are defined as a function of the wind velocity at 20 feet. In this work, however, we can use the CFD results directly to compute the root-mean-square of the velocity intensity $\sigma = \sigma_u = \sigma_v = \sigma_w$ based on the TKE values k at every point in the 3D domain from

$$\sigma = \sigma_u = \sigma_v = \sigma_w = u' = \sqrt{\frac{1}{3}(u_x'^2 + u_y'^2 + u_z'^2)} = \sqrt{\frac{2}{3}k} \quad (9)$$

The turbulence length scale L in equations (7)-(8) is typically approximated as simply the height of the UAV for low altitude situations less than 300 m [26]. The above relations are valid for single point analyses, however, if we are interested in analysing the 3D representation of the atmospheric turbulence field, we can extend the approach following [28] to include the spatial cross-correlations in the turbulence spectra.

The Dryden spectrum is defined in equations (7)-(8) in terms of reduced frequencies ω . To obtain the temporal representation, a continuous forming filter based on the Dryden spectrum is typically used [26]. By driving the Dryden filter with a unit variance, white noise signal we can obtain a random time history that follows the Dryden spectrum. Alternatively, we can obtain the time history of the gust velocities, $G_{u,v,w}$, in 3D efficiently through an inverse Fourier transform of equations (7)-(8), as

$$G_{u,v,w}(t) = \sum_{m=1}^{\infty} \sqrt{\Phi_{u,v,w}(\omega_m)\Delta\omega} \cos(\omega_m t + \psi_m) \quad (10)$$

where the phase angle $-\pi \leq \psi_m < \pi$ is generated as a random process to encapsulate the random nature in the disturbance signal. The longitudinal, lateral and vertical velocities, G_u, G_v and G_w , can be inputted directly in a UAV dynamics model as an external flow disturbance. As proposed in [1], we can then determine critical levels of TKE based on the UAV simulation. The results can be used to either tune the UAV control system or completely avoid areas of high TKE for a safe UAV operation. The latter approach links directly to research in UAV path planning and obstacle avoidance where high TKE areas can be considered as obstacles.

The simulations in [1] determined an operating limit for TKE values of 6 J/kg for the specific UAV used in the study. As seen from the TKE contours in Figure 11, the highest TKE value is 2 J/kg in the current AIJ study. For this urban scenario, the UAV is able to safely operate for this particular wind direction at a height 10m. However, different UAV designs react very differently to gust disturbances and will exhibit different TKE limits. The proposed CFD-based simulation approach for highly complex urban environments therefore provides a fast and stable method to generate the flow field. The approach can be used to test the effect of different wind directions or investigate the alleviating effects of changes in the building geometries.

4 Conclusions and Future Work

Usage of full scale highly detailed complex urban geometries is now possible due to the increase in available and accessible computational power. The use of a cloud-based CFD solver to perform analysis for otherwise very computationally expensive cases is key factor in further development and understanding of CWE for practical uses. Several points can be concluded from the investigation:

1. The performance between the $k-\epsilon$ and $k-\omega$ SST turbulence models for overall prediction accuracy is similar for a highly complex urban geometry. However, the $k-\epsilon$ model underpredicts at more points than the $k-\omega$ SST model. For applications to UAV pathing where underprediction is less desirable than overprediction, the $k-\omega$ SST model is deemed as better performing.
2. Result accuracy can be better improved should additional attention be paid to creation of the mesh. Areas that contain complex flow interaction which includes features such as ground elevation and non-regular structures will need higher mesh qualities in order to deduce accurate data. Ensuring sufficient mesh quality at these areas would also ensure that flow effects can be captured that will affect the accuracy of prediction downstream.
3. With the translation of a steady-state data to a representative transient one, further prediction accuracy can be gained especially towards applications for UAV path optimization. Usage of such a method can also be applied for other CWE analysis where usage steady-state data is not sufficient, yet fully transient simulations are not economical.

Future studies should investigate other or all available wind directions if possible to further validate the conclusions drawn from this study. Additionally, other types of turbulence models can use the same approach from this study in order to assess their performance. Suggestions for other turbulence models include but are not limited to RNG $k-\epsilon$, realizable $k-\epsilon$ or even hybrid LES. It should be noted that LES may still be too computationally expensive to be used with a mesh of this size.

Inclusion of details like thermal effects and geometrical details such as trees or small obstacles may affect the results and prediction accuracy to varying degrees. As such in future studies consideration or inclusion of such effects should be assessed to determine the amount of influence they have.

References

- [1] C. W. A. Murray and D. Anderson, 'A CFD based procedure for airspace integration of small unmanned aircraft within congested areas', *Int. J. Micro Air Veh.*, vol. 9, no. 4, pp. 235–252, Dec. 2017.
- [2] W. D. Janssen, B. Blocken, and T. van Hooff, 'Pedestrian wind comfort around buildings: Comparison of wind comfort criteria based on whole-flow field data for a complex case study', *Build. Environ.*, vol. 59, pp. 547–562, Jan. 2013.
- [3] B. Blocken, '50 years of Computational Wind Engineering: Past, present and future', *J. Wind Eng. Ind. Aerodyn.*, vol. 129, pp. 69–102, Jun. 2014.
- [4] Y. Tominaga *et al.*, 'AIJ guidelines for practical applications of CFD to pedestrian wind environment around buildings', *J. Wind Eng. Ind. Aerodyn.*, vol. 96, no. 10, pp. 1749–1761, Oct. 2008.
- [5] T. van Hooff, B. Blocken, and Y. Tominaga, 'On the accuracy of CFD simulations of cross-ventilation flows for a generic isolated building: Comparison of RANS, LES and experiments', *Build. Environ.*, vol. 114, pp. 148–165, Mar. 2017.
- [6] T. van Hooff and B. Blocken, 'Coupled urban wind flow and indoor natural ventilation modelling on a high-resolution grid: A case study for the Amsterdam ArenA stadium', *Environ. Model. Softw.*, vol. 25, no. 1, pp. 51–65, Jan. 2010.
- [7] A. Mochida and I. Y. F. Lun, 'Prediction of wind environment and thermal comfort at pedestrian level in urban area', *J. Wind Eng. Ind. Aerodyn.*, vol. 96, no. 10, pp. 1498–1527, Oct. 2008.
- [8] T. Tamura, 'Towards practical use of LES in wind engineering', *J. Wind Eng. Ind. Aerodyn.*, vol. 96, no. 10, pp. 1451–1471, Oct. 2008.
- [9] B. Blocken, 'Computational Fluid Dynamics for urban physics: Importance, scales, possibilities, limitations and ten tips and tricks towards accurate and reliable simulations', *Build. Environ.*, vol. 91, pp. 219–245, Sep. 2015.
- [10] R. Yoshie *et al.*, 'Cooperative project for CFD prediction of pedestrian wind environment in the Architectural Institute of Japan', *J. Wind Eng. Ind. Aerodyn.*, vol. 95, no. 9, pp. 1551–1578, Oct. 2007.
- [11] Y. S. Chen and S. W. Kim, 'Computation of turbulent flows using an extended k- ϵ turbulence closure model', *NASA STIRecon Tech Rep N*, vol. 88, p. 11969, 1987.
- [12] F. R. Menter, 'Two-equation eddy-viscosity turbulence models for engineering applications', *AIAA J.*, vol. 32, no. 8, pp. 1598–1605, Aug. 1994.
- [13] B. Blocken, T. Stathopoulos, and J. P. A. J. van Beeck, 'Pedestrian-level wind conditions around buildings: Review of wind-tunnel and CFD techniques and their accuracy for wind comfort assessment', *Build. Environ.*, vol. 100, pp. 50–81, May 2016.
- [14] H. Cheng-Hu, T. Kurabuchi, and M. Ohba1, 'Numerical Study of Cross-Ventilation Using Two-Equation RANS', *Int. J. Vent.*, vol. 4, no. 2, pp. 123–131, Sep. 2005.
- [15] J. I. Perén, T. van Hooff, B. C. C. Leite, and B. Blocken, 'CFD simulation of wind-driven upward cross ventilation and its enhancement in long buildings: Impact of single-span versus double-span leeward sawtooth roof and opening ratio', *Build. Environ.*, vol. 96, pp. 142–156, Feb. 2016.
- [16] J. I. Perén, T. van Hooff, B. C. C. Leite, and B. Blocken, 'Impact of eaves on cross-ventilation of a generic isolated leeward sawtooth roof building: Windward eaves, leeward eaves and eaves inclination', *Build. Environ.*, vol. 92, pp. 578–590, Oct. 2015.
- [17] J. I. Perén, T. van Hooff, R. Ramponi, B. Blocken, and B. C. C. Leite, 'Impact of roof geometry of an isolated leeward sawtooth roof building on cross-ventilation: Straight, concave, hybrid or convex?', *J. Wind Eng. Ind. Aerodyn.*, vol. 145, pp. 102–114, Oct. 2015.
- [18] J. I. Perén, T. van Hooff, B. C. C. Leite, and B. Blocken, 'CFD analysis of cross-ventilation of a generic isolated building with asymmetric opening positions: Impact of roof angle and opening location', *Build. Environ.*, vol. 85, pp. 263–276, Feb. 2015.
- [19] R. Ramponi and B. Blocken, 'CFD simulation of cross-ventilation flow for different isolated building configurations: Validation with wind tunnel measurements and analysis of physical and numerical diffusion effects', *J. Wind Eng. Ind. Aerodyn.*, vol. 104–106, pp. 408–418, May 2012.

- [20] R. Ramponi and B. Blocken, ‘CFD simulation of cross-ventilation for a generic isolated building: Impact of computational parameters’, *Build. Environ.*, vol. 53, pp. 34–48, Jul. 2012.
- [21] BCA, ‘BCA GreenMark Non-Residential Buildings NRB: 2015 Technical Guide and Requirements’. Building Construction Authority, 02-Nov-2016.
- [22] R. Britter and M. Schatzmann, ‘COST 732: The model evaluation guidance and protocol document’, *Univ. Hambg. Meteorol. Inst. Cent. Mar. Atmospheric Sci.*, Apr. 2018.
- [23] P. Yao, H. Wang, and Z. Su, ‘UAV feasible path planning based on disturbed fluid and trajectory propagation’, *Chin. J. Aeronaut.*, vol. 28, no. 4, pp. 1163–1177, Aug. 2015.
- [24] F. M. Hoblit, *Gust Loads on Aircraft: Concepts and Applications*. American Institute of Aeronautics and Astronautics, 1988.
- [25] B. F. Ng, H. Hesse, R. Palacios, J. M. R. Graham, and E. C. Kerrigan, ‘Aeroservoelastic state-space vortex lattice modeling and load alleviation of wind turbine blades’, *Wind Energy*, vol. 18, no. 7, pp. 1317–1331.
- [26] S. Gage, ‘Creating a Unified Graphical Wind Turbulence Model from Multiple Specifications’, in *AIAA Modeling and Simulation Technologies Conference and Exhibit*, 0 vols, American Institute of Aeronautics and Astronautics, 2003.
- [27] ‘The Code of Federal Regulations of the United States of America, Title 14: Aeronautics and Space, Part 25 -- Airworthiness Standards: Transport Category Airplanes’. Federal Aviation Administration, 2007.
- [28] J. Gao and G. Hong, ‘Numerical simulation for 3D atmospheric turbulence field’, in *2016 7th International Conference on Mechanical and Aerospace Engineering (ICMAE)*, 2016, pp. 304–308.